



Estimation of chlorophyll a content in inland turbidity waters using WorldView-2 imagery: a case study of the Guanting Reservoir, Beijing, China

Xing Wang · Zhaoning Gong · Ruiliang Pu

Received: 2 March 2018 / Accepted: 13 September 2018 / Published online: 29 September 2018
© Springer Nature Switzerland AG 2018

Abstract Complex optical properties, such as non-pigment suspension and colored dissolved organic matter (CDOM), make it difficult to achieve accurate estimations of remotely sensed chlorophyll a (Chla) content of inland turbidity. Recent attempts have been made to estimate Chla based on red and near-infrared regions where non-pigment suspension and CDOM have little effect on water reflectance. The objective of this study is to validate the applicability of WV-2 imagery with existing effective estimation methods from MERIS when estimating Chla content in inland turbidity waters. The correlation analysis of measured Chla content and WV-2 imagery bands shows that the Chla sensitive bands of WV-2 are red edge, NIR 1, and NIR 2. The coastal band is designed for seawater Chla detection. However, the high correlation with turbidity data and low correlation with Chla made coastal band unsuitable for estimating Chla in inland waters. The high-resolution water body images were extracted by combining the spectral products (NDWI) with the spatial morphological products (sobel edge detection). The estimation results show that the accuracy of the single band and NDCI is not as good as the two-band method, three-band method, stepwise regression algorithm

(SRA) and support vector machines (SVM). The SVM estimation accuracy was the highest with an R^2 , RMSE, and URMSE of 0.8387, 0.4714, and 19.11%, respectively. This study demonstrates that the two-band and three-band methods are effective for estimating Chla in inland water for WV-2 imagery. As a high-precision estimation method, SVM has great potential for inland turbidity water Chla estimation.

Keywords Inland turbid waters · WV-2 imagery · Red edge · Sobel edge detection · Chlorophyll a estimation algorithms · SVM

Introduction

Accurate estimations of biophysical parameters, such as chlorophyll a (Chla), are essential for studies on water quality. Chla is an important pigment for the photosynthesis of algae and can be used to gauge the overall content of algae and assess nutritional status. Water spectral reflectance ($Rrs(\lambda)$) detected by remote sensors provides qualitative information on optically significant materials present in natural water. The highly variable composition of constituents in inland waters creates reliability issues when interpreting the optical information from water surface reflectance (Yacobi et al. 2011).

Empirical algorithms that use the blue and green part of the electromagnetic spectrum, e.g., OC4v4, provide a relatively accurate estimate of Chla in case 1 waters where the total non-water absorption is dominated by phytoplankton (Gordon and Morel 1983; O'Reilly et al.

X. Wang · Z. Gong (✉)
College of Resource Environment & Tourism, Capital Normal University, Beijing 100048, China
e-mail: gongznh@163.com

R. Pu
School of Geosciences, University of South Florida, 4202 E. Fowler Ave., Tampa, FL 33620, USA

1998), but are not suitable for inland waters heavily affected by constituents, such as Color Dissolved Organic Matter (CDOM), detritus, and phytoplankton. In the past decade, a variety of algorithms have been developed to reduce the estimation error of Chla in turbid inland waters. Almost all the algorithms are based on the red and near-infra-red (NIR) regions, where absorption of non-algal particles and CDOM largely fade in those portions of the electromagnetic spectrum (Gitelson 1992; Gons 1999; Schalles 2006). Gons (1999) first used the reflectance ratio of 704 to 672 nm and the absorption at these wavelengths to estimate Chla concentration. Gons et al. (2005) adapted his algorithm for use with MERIS by using 708 to 665 nm and reported high accuracy of Chla concentration estimation. Jiao et al. (2006) estimated Chla concentration in Taihu Lake using the ratio of 705 to 678 nm. These algorithms all assume that optical parameters, such as Chla-specific absorption coefficient and Chla fluorescence quantum yield, remain constant, which have a considerable impact on their accuracy (Dall'Olmo and Gitelson 2005, 2006). Han and Rundquist (1997) compared the NIR/Red ratio and first derivative of reflectance to estimate Chla concentration. First derivative of reflectance algorithm is only able to remove the effects of pure water (Goodin et al. 1993). Suspended solids and dissolved matter concentration limit the estimation accuracy; first derivative of reflectance algorithm is inapplicable to inland turbid water (Le et al. 2009).

Recently, the semi-analytical method based on the mechanism of water color has been widely used in the study of Chla estimation. Dall'Olmo et al. (2005) and Gitelson et al. (2008) used the three-band semi-analytical algorithm to estimate Chla concentration in turbid water. This three-band semi-analytical algorithm, $C_{\text{chl-a}} \propto [Rrs^{-1}(665) - Rrs^{-1}(708)] \times Rrs(753)$ may violate three assumptions of 665, 708, and 753 in highly turbid waters. Le et al. (2009) improved the three-band semi-analytical algorithm using a proposed four-band semi-analytical algorithm that increases the accuracy for estimating Chla in highly turbid waters.

The objective of this study is to validate the existing Chla estimation algorithms based on high-resolution multispectral images from WorldView-2 rather than MODIS and MERIS for the Guanting Reservoir. The specific goals are (1) to locate the optimal spectral positions of the two-band ratio approach and the three-band semi-analytical approach, (2) to evaluate the

accuracy of normalized difference chlorophyll index (NDCI) (Mishra and Mishra 2012) for accurately estimating Chla in the Guanting Reservoir, (3) to develop stepwise regression analysis algorithm (SRA) for estimating Chla in inland water, (4) to develop support vector machines (SVM) model for estimating Chla, and (5) to select the best algorithm for the Guanting Reservoir by comparing the accuracy of different Chla estimation algorithms in inland turbidity waters.

Study area and data sets

Study area

Guanting Reservoir is the first large-scale reservoir, located between $40^{\circ} 18' - 40^{\circ} 26' \text{ N}$ and $115^{\circ} 37' - 115^{\circ} 51' \text{ E}$, built after the establishment of new China (Figs. 1 and 2). Its total storage capacity is 4.16 billion m^3 ; the total area of the reservoir basin is $43,400 \text{ km}^2$, the average annual flow is $44.6 \text{ m}^3 \text{ s}^{-1}$, and the average depth of Guanting Reservoir is about 7.6 m (Zhen et al. 2012; Zhu et al. 2015). Guanting Reservoir plays an important role in flood control, agricultural irrigation, and energy supply for many provinces and cities; it was one of the main water supply sources in Beijing. However, in the late 1980s, the reservoir area became severely polluted and the water quality continued to deteriorate into the 1990s. In 1997, the reservoir was forced to withdraw from the urban drinking water system. After effective protection and restoration, the water quality of the reservoir improved, and it reopened in 2007. Due to the long-term interaction of the unique geographical environment, water quality conditions and climatic conditions, Guanting Reservoir serves as a biodiversity hotspot for an abundance of wet plants like phragmites and *Potamogeton pectinatus*.

Data sets

Field data collection

We conducted water quality sampling on the upper reaches of Guanting Reservoir on July 11, 2016. The 40 sample points were evenly distributed along the south bank, north bank, and midline areas of the reservoir (Fig. 1). Reflectance measurements and water quality sampling was performed between 10:00 and 14:00 h local time (Le et al. 2009). Measurement data requires

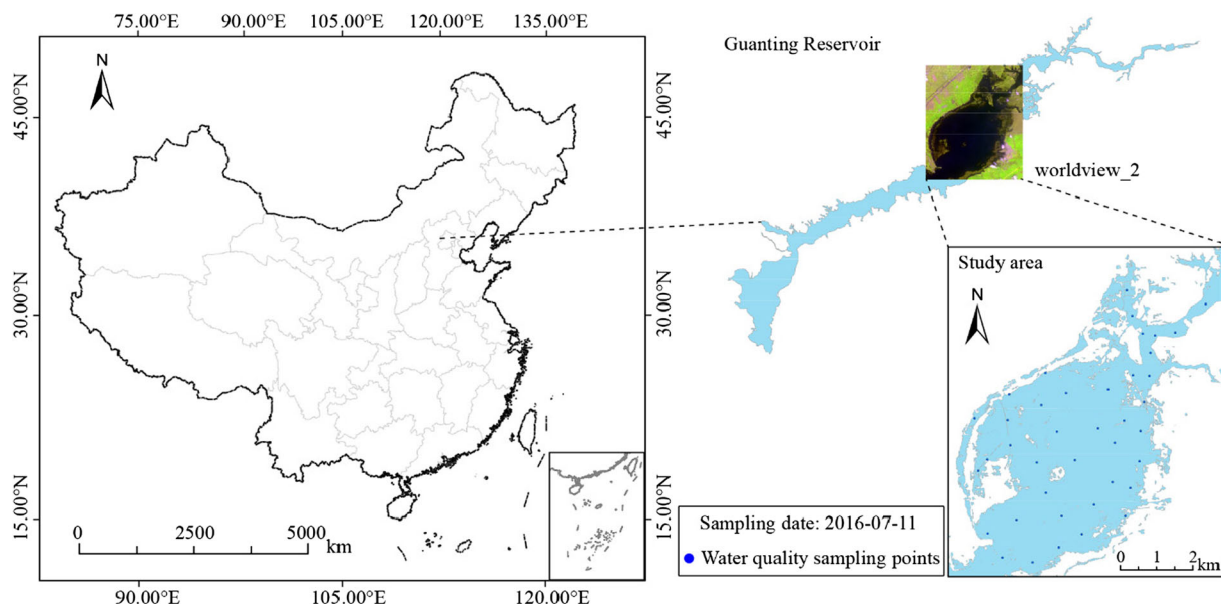


Fig. 1 Location of Guanting Reservoir and study site and spatial distribution of water quality sampling points

relatively calm water, sunny weather, and low cloud cover. We used a handheld GPS to obtain the sampling points' latitude and longitude; we used the portable water quality analyzer, Hydrolab DS5x, to collect chlorophyll a concentration, pH value, water temperature, and other data; and the portable turbidity meter, HAN-NA (HI93703-11), to measure the turbidity at each sampling point. Turbidity value is determined by the scattering of light caused by small particles in water. Hydrolab used fluorescence method to measure the content of Chla in water. The probe emits light with a wavelength of 460 nm into the water, where chlorophyll absorbs energy from it and emits fluorescence with a wavelength of 620–715 nm. The ASD Company's

FieldSpec3 back-hanging field hyperspectral radiometer was used to collect samples of measured spectra. The instrument can measure continuously in the 350–2500 nm wavelength range, with a spectral resolution of 3 nm, a sampling interval of 1.4 nm, a fiber front field angle of 25°.

There is a notable difference in the spectra of water and plants. Spectral measurements of plants can be obtained by directly measuring the relative reflectivity through whiteboard calibration. The spectral characteristics of the water contain apparent optical properties (AOPs) and intrinsic optical characteristics (IOPs) (Mobley 1994). In this paper, water spectrum measurement method is the apparent spectral measurement. In

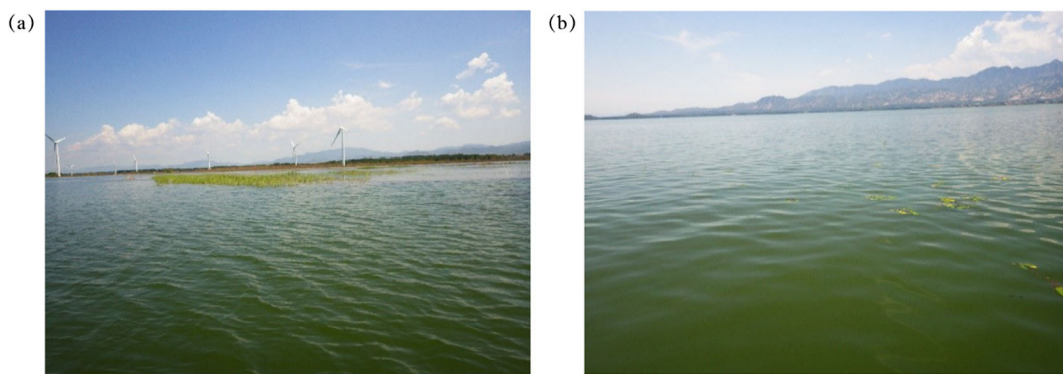
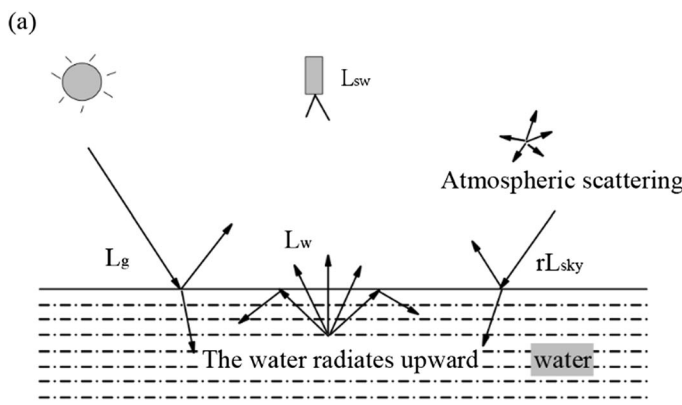


Fig. 2 Photos of Guanting Reservoir

case 1 waters, the profiling method is preferred for the international ocean color remote sensing sector; in case 2 waters, the only effective method is the above-water method (Tang et al. 2004). The source and composition of the above-water signal are shown in Fig. 3a. Where L_{sw} represents the instrument receives total radiation; rL_{sky} represents the sky light reflection; L_w represents the radiation from the water; L_g represents the direct reflection of the sun. When measuring the water spectrum, we calculate signal values of the spectrometer for the water, the sky, and the standard plate, respectively. To avoid the effects of ship shadows on the surface and direct solar radiation during the measurement process, we kept the instrument on the ship deck about 1 m from the water. The instrument was positioned at the back to the sun's incident radiation plane angle ϕ_v , 90° – 135° ; and the angle between the instrument and the sea normal direction $30^\circ \leq \theta_v \leq 45^\circ$ (Fig. 3b). For non-strictly calibrated spectrometers, the remote sensing reflectance can be calculated directly according to Eq. (1):

$$R_{rs} = \frac{[S_{sw} - rS_{sky}]\rho_p}{\pi S_p} \quad (1)$$

where S_{sw} represents the measured signal value of the spectrometer facing the water; S_{sky} is the measured signal value of the spectrometer facing the sky; S_p is the measured signal value of the spectrometer facing the standard board; the value of R_{rs} is generally less than 0.051. According to Tang et al. (2004) and other experience in water measurement and analysis, the calm water surface value for r is 2.2% for the above observation conditions. At about 5 m/s wind speed, r equals 0.025; at about 10 m/s wind speed, r is between 0.026 and 0.028.



WorldView-2

A WorldView-2 (WV2) image taken at UTC time 03:23:32.14 on July 17, 2016, only 6 days after our water measurements were collected was used for this study. WV2 is the first commercial high-resolution satellite sensor with eight multispectral bands (Pu and Landry 2012). WorldView-2 was launched on October 6, 2009 to produce 0.5-m panchromatic images and multispectral images at 1.8-m resolution. The development of quantitative remote sensing not only improved spatial details but also preserved the spectral information of multispectral bands. The WV2 sensor provides a high-resolution panchromatic band and eight multispectral bands; four standard colors (red, 630–690 nm; green, 510–580 nm; blue, 450–510 nm; and near-infrared 1 (NIR 1), 770–895 nm) and four new bands (coastal, 400–450 nm; yellow, 585–625 nm; red edge, 705–745 nm; and near-infrared 2 (NIR 2), 860–1040 nm). The full-color images can be used for enhanced spectral analysis, mapping, and monitoring applications, land-use planning, disaster relief, exploration, defense and intelligence, and visualization and simulation environments (DigitalGlobe 2009).

Methods

Analysis of water spectral reflectance characteristics

Due to outside factors, like the spectral characteristics of the measuring instrument or target itself, influencing spectral measurements, the data may contain a large amount of noise. This requires the use of spectral data

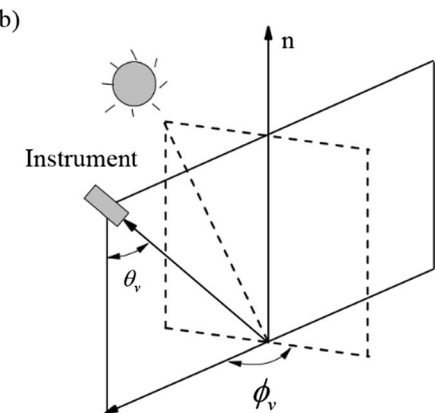


Fig. 3 **a** Above water signal composition (from Kirk 1994). **b** Viewing geometry of the above-water measurement (from Tang et al. 2004)

pretreatment to eliminate noise interference and highlight the target spectrum.

The preprocessing of spectral data involves spectral smoothing and denoising, eliminating water vapor absorption bands, and spectral curve mean processing. The filtered spectral value is expressed by averaging the value of nine bands before and after each value:

$$R'_i = (R_{i-4} + R_{i-3} + R_{i-2} + R_{i-1} + R_i + R_{i+1} + R_{i+2} + R_{i+3} + R_{i+4})/9 \quad (2)$$

After 1000 nm, the spectral curve of water vapor noise is obvious. Considering the combination of image band analysis, we chose 350–1000 nm for research. The average of ten spectral curves at each sample point was calculated and used as the sample value.

The sensitive bands of Chla were found by calculating the Pearson correlation coefficient (r) (Wang 2013) between water reflectance and measured Chla concentration. The expression for r is:

$$r = \frac{N\sum x_i y_i - \sum x_i \sum y_i}{\sqrt{N\sum x_i^2 - (\sum x_i)^2} \sqrt{N\sum y_i^2 - (\sum y_i)^2}} \quad (3)$$

where x and y represent the two groups of variables in the correlation analysis.

WV2 processing and water body extraction

The original WorldView-2 multispectral image is delivered in 16-bit formatted digital number (Lin et al. 2015). FLAASH (Fast Line-of-sight Atmospheric Analysis of Spectral Hypercube), ENVI's atmospheric correction algorithm based on MODTRAN4 code, was also applied to the image data. The required sensor spectral response function was kindly provided by Digital Globe (Manakos et al. 2011). The FLAASH module has proven successful for the atmospheric correction of multispectral images. The “Pan Sharpening” method, using Gram-Schmidt's algorithm bundled in the ENVI software, is applied for image fusion (Laben and Brower 2000).

High-resolution remote sensing images have obvious spectral characteristics and rich information, such as texture and shape. They must only rely on spectral characteristics of the target expression, otherwise feature classification results are less reliable. In order to make use of the spatial structure of high-resolution images, this study makes an edge feature extraction. The

detection of edge lines in the image is the basis of image segmentation and feature extraction. Sobel operator, one of the most practical edge extraction algorithms, is applied for this study.

Consequently, in processing, we used adjacent or spaced pixel differential values to represent the edge information of the image. The image band extracted by the Sobel edge feature was stacked with the (normalized difference water index) NDWI (Mcfeeters 1996) layer of the original image, followed by image segmentation to establish the classification rule (Fig. 4).

Chla content retrieval algorithms

Single-band and band ratio approach

Single-band approach can be expressed as follows:

$$C_{\text{chl}a} \propto Rrs(\lambda) \quad (4)$$

where $C_{\text{chl}a}$ is the estimated concentration of Chla, and λ is the band having a high correlation with the Chla concentration. According to the results of Fig. 6b, it can be found that the correlation between Chla and the red edge (band 6) of the WorldView-2 is high, with a coefficient of 0.895.

Two-band ratio approach

Two-band ratio approach can be expressed as follows:

$$C_{\text{chl}a} \propto Rrs(\lambda_1)/Rrs(\lambda_2) \quad (5)$$

The two-band ratio approach partially eliminates the interference of environmental factors such as smoothness of water surface and tiny waves, and reduces the effects of other non-target substances (Duan et al. 2006). It broadens the difference between chlorophyll absorption peak and reflection or fluorescence peak and extracts information on Chla concentration (Zhou et al. 2004). We found that when $Rrs(\lambda_1)$ and $Rrs(\lambda_2)$ represent the red edge band and green band respectively, the ratio of them is highly correlated with Chla in this study (Fig. 7a).

Three-band approach

Since the absorption of CDOM and debris particles in the red and NIR bands cannot be ignored when estimating chlorophyll a in turbid waters, Dall'Olmo

et al. (2005) and Gitelson et al. (2008) developed a three-band approach that can be expressed as follows:

$$C_{\text{chl}a} \propto \left[\text{Rrs}(\lambda_1)^{-1} - \text{Rrs}(\lambda_2)^{-1} \right] \times \text{Rrs}(\lambda_3) \quad (6)$$

Where λ_1 is the most sensitive area for Chla absorption; λ_2 is the fluorescence peak region of Chla; λ_3 is influenced by backscattering only, with minimal influence from water constituent absorption. And we found that $\text{Rrs}(\lambda_1)$, $\text{Rrs}(\lambda_2)$, and $\text{Rrs}(\lambda_3)$ represent the red band, red edge band, and NIR1 band respectively in this study, three-band approach worked best in Chla estimation.

Normalized difference chlorophyll index (NDCI)

Mishra and Mishra (2012) proposed a normalized difference chlorophyll index (NDCI) to estimate Chla concentration from remotely sensed data in coastal and estuarine turbid waters (case 2). It was then tested for accuracy and its potential to become as widely applicable as NDVI.

The NDCI approach can be expressed as follows:

$$C_{\text{chl}a} \propto \frac{[\text{Rrs}(708) - \text{Rrs}(665)]}{[\text{Rrs}(708) + \text{Rrs}(665)]} \quad (7)$$

According to the WorldView-2 image band characteristics, NDCI can be expressed as follows:

$$C_{\text{chl}a} \propto \frac{[\text{RedEdge} - \text{Red}]}{[\text{RedEdge} + \text{Red}]} \quad (8)$$

Stepwise regression analysis algorithm (SRA)

The objective of stepwise regression is to introduce variables one by one into the model. Each time an explanatory variable is introduced, an F test must be carried out. The explanatory variables that have been selected must then be checked individually. With a new explanatory variable introduced, the previous explanatory may lose their predictive ability, and can be deleted (Chen et al. 2013).

Support vector machines (SVM)

A support vector machine maps the input vector to a high-dimensional space through nonlinear mapping, and then constructs an optimal hyperplane in high-dimensional

space (Sun et al. 2009). By using the kernel function, it avoids the non-linear mapping of the display and overcomes computational difficulties caused by the high-dimensional space, and provides a new solution for the nonlinear regression problem. Support vector machines have many unique advantages in solving small sample, nonlinear, and high-dimensional pattern recognition problems. In principle, it should solve a quadratic programming problem, with the advantages of strong generalization ability, easy training, and no local minima (for a more detailed algorithm, see Vapnik 1996; Wang et al. 2009).

Accuracy assessment

In this study, Chla algorithm performance and product uncertainties at pixel level were assessed by a determination coefficient (R^2), root-mean-square-error (RMSE), and unbiased RMSE (URMSE) in relative percentage (100%) (Zhang et al. 2016).

$$R^2 = 1 - \frac{\sum_{i=1}^n (y_i - \hat{y}_i)^2}{\sum_{i=1}^n (y_i - \bar{y})^2} \quad (9)$$

$$\text{RMSE} = \sqrt{\frac{\sum_{i=1}^n (y_i - \hat{y}_i)^2}{n}} \quad (10)$$

$$\text{URMSE} = \sqrt{\frac{\sum_{i=1}^n \left(\frac{y_i - \hat{y}_i}{0.5(y_i + \hat{y}_i)} \right)^2}{n}} \times 100\% \quad (11)$$

where y_i and \hat{y}_i are the measured and predicted values for the Chla sample points, and \bar{y} refers to the average of measured values. The use of URMSE in addition to the typical RMSE was proposed by Hooker et al. (2002) and used to avoid the impact of outliers causing skewed error distributions. When $p \leq 0.05$, it is considered to be statistically significant.

Results and analyses

Water spectral reflectance characteristics

Following spectral pretreatment and remote sensing reflectance calculation, the above-water remote sensing reflectance is shown in Fig. 5.

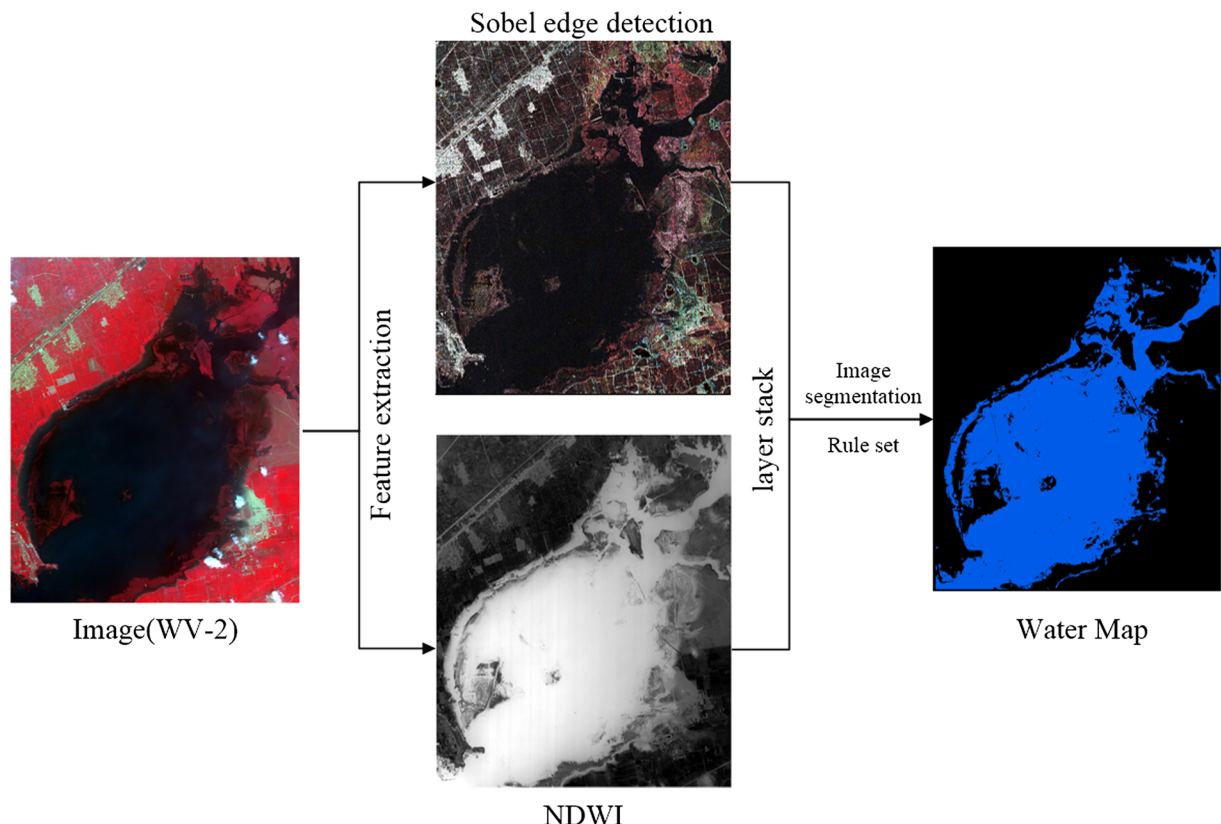
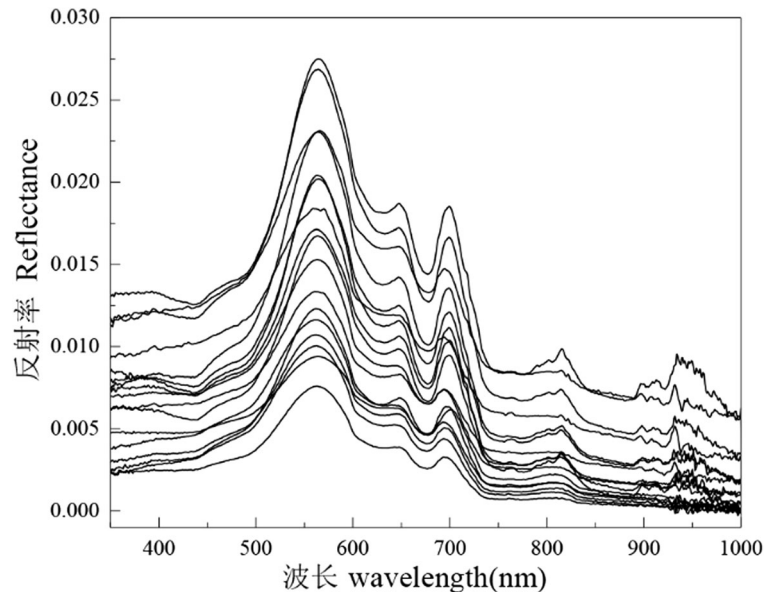


Fig. 4 High-resolution image water extraction method

The results of the above-water remote sensing reflectance measurements (Fig. 5) indicate that the spectral reflectance exhibits the general characteristics of inland

water. In the range of 400–500 nm, Chla and CDOM are strongly absorbed, resulting in low reflectivity of water bodies. Due to the weak absorption of Chla, carotene

Fig. 5 Above-water remote sensing reflectance ($Rrs(\lambda)$, $N=17$) measured in Quanting Reservoir



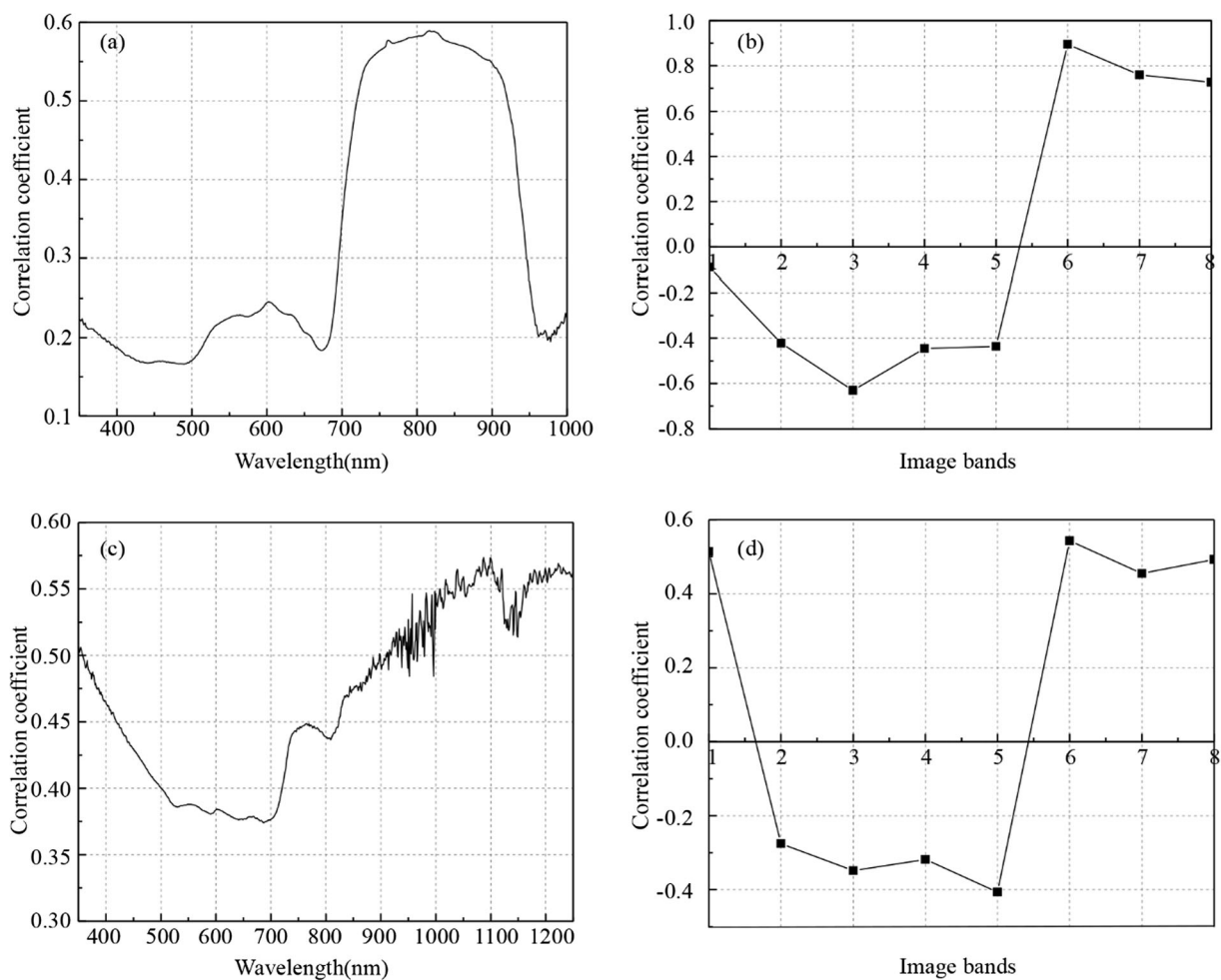


Fig. 6 **a** The correlation coefficient of Chla concentration and spectral normalized reflectivity of water measured by ASD. **b** The correlation curve of Chla concentration and image bands. **c** The correlation coefficient of turbidity concentration and spectral normalized reflectivity of water measured by ASD. **d** The correlation curve of turbidity concentration and image bands

correlation coefficient of turbidity concentration and spectral normalized reflectivity of water measured by ASD. **d** The correlation curve of turbidity concentration and image bands

and cell scattering effects result in a significant reflection peak near 540 nm. The most significant spectral characteristic of algae-filled water is the reflection peak at 690 nm—its presence determines if there is algal Chla in the water. Due to the absorption of pure water in the infrared band, the spectral curve decreased dramatically in the 730–900 nm longwave reflectivity.

The correlation coefficient between the measured concentration of Chla in Guanting Reservoir and the reflectivity of water in each band shows that the correlation is low for wavelengths between 350 and 680 nm, with the coefficient at about 0.2; however, in the wavelength range of 680–750 nm, the correlation between them significantly improves (Fig. 6a). In the wavelength range of 750–800 nm, the correlation between them is the strongest, at 0.6. The correlation coefficient between

the measured concentration of Chla and the WorldView-2 image indicates that the correlation between Chla concentration and the red and near infrared bands (6, 7, and 8) was the best (Fig. 6b). The Chla concentration has the lowest correlation with the coastal band of the image (band 1).

The correlation coefficient of the measured turbidity data of Guanting Reservoir and the reflectivity of water in each band shows that the correlation coefficient is higher than 0.5 at the 400-nm wavelength, and the correlation between the two decreases as wavelength increases from 400 to 700 nm. For wavelengths above 700 nm, the correlation between the two increases as wavelength increases (Fig. 6c). The correlation coefficient between the turbidity data and the WorldView-2 image shows that in the Coastal,

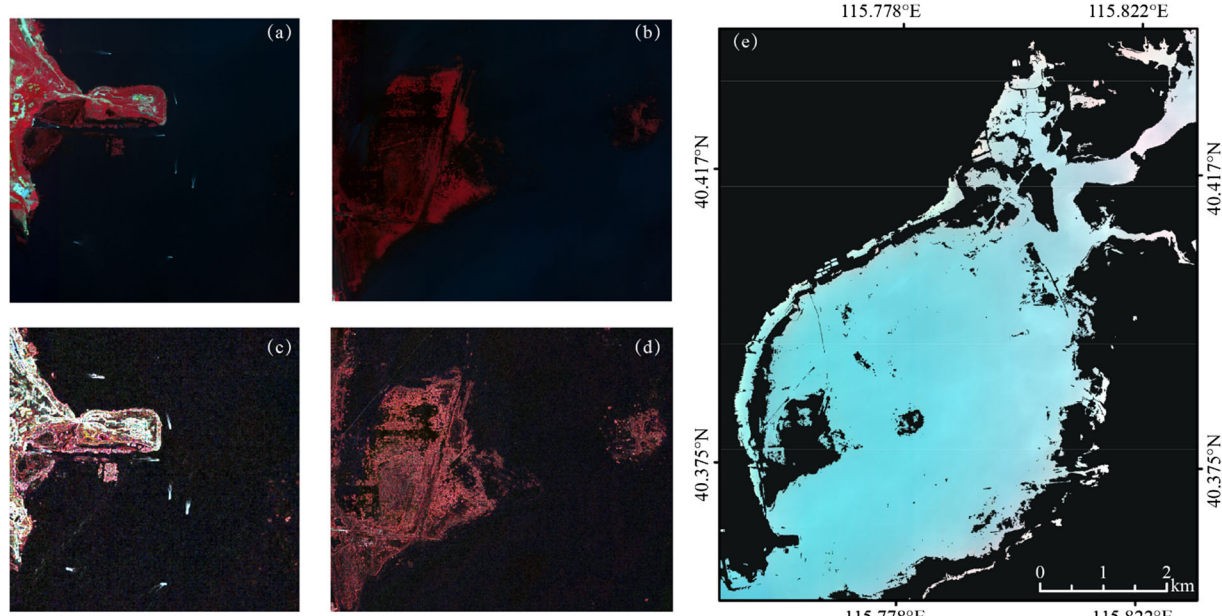


Fig. 7 **a, b** WV-2 original image. **c, d** Sobel algorithm edge feature extraction results. **e** WV-2 image water extraction result

red edge and near infrared band, they are highly correlated, with the coefficient being greater than 0.5 (Fig. 6d).

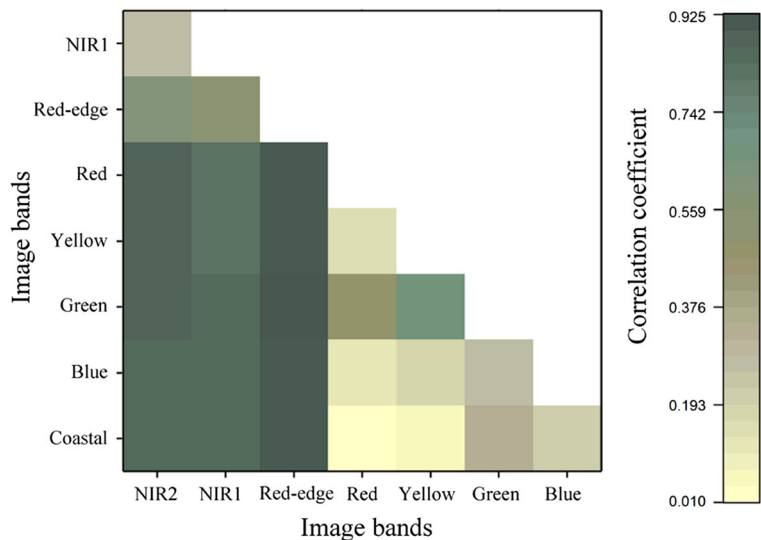
Based on the above four graphs, it can be concluded that the concentration of chlorophyll a in the turbid water of the Guanting Reservoir has a good correlation in the infrared and near infrared bands. The coastal band of WorldView-2 supports plant identification and analysis and also supports the study of deep-sea exploration based on chlorophyll. But the correlation between Chla

and coastal band is low in inland turbid water. Therefore, coastal band is not suitable for estimating chlorophyll a in inland waters.

Water body extracted by WV-2.

The results of the water body extraction using the Sobel edge detection algorithm and normalized difference water index, NDWI, are shown below (Fig. 7). High-resolution images can distinguish aquatic plants from relatively pure

Fig. 8 Correlation coefficient of WV-2 image band ratio and Chla



water more accurately than medium-resolution images from MODIS or MERIS. Removing the effects of aquatic plants improves the accuracy of Chla estimation. Object-oriented classification method was used to extract water, and the result of water is shown in Fig. 7e.

Chla content retrieval results

The six approaches (single-band approach, two-band ratio approach, three-band approach, NDCI, stepwise regression analysis algorithm, and SVM) were all assessed for measured data corresponding to WV-2 bands. The positions determined by the correlation between measured Chla and the bands were adjusted for the WV-2 image by selecting the corresponding bands.

Due to the different biological optical variability of different water bodies, such as Chla-specific absorption coefficient (Dall'Olmo and Gitelson 2005), these band position approaches are all region-dependent.

We determined the band selection for the single-band approach by analyzing the correlation between the measured chlorophyll a and the WV-2 image bands (Fig. 6b). For the single-band approach, red edge was chosen because of its high correlation. The small number of WV-2 image bands enabled us to correlate the two band ratio results with the measured chlorophyll a (Fig. 8). The band selection of the three band approaches is relatively easy to determine on the WV-2 image. When NIR2 is selected as λ_3 , the correlation between the three band approaches and chlorophyll a is highest.

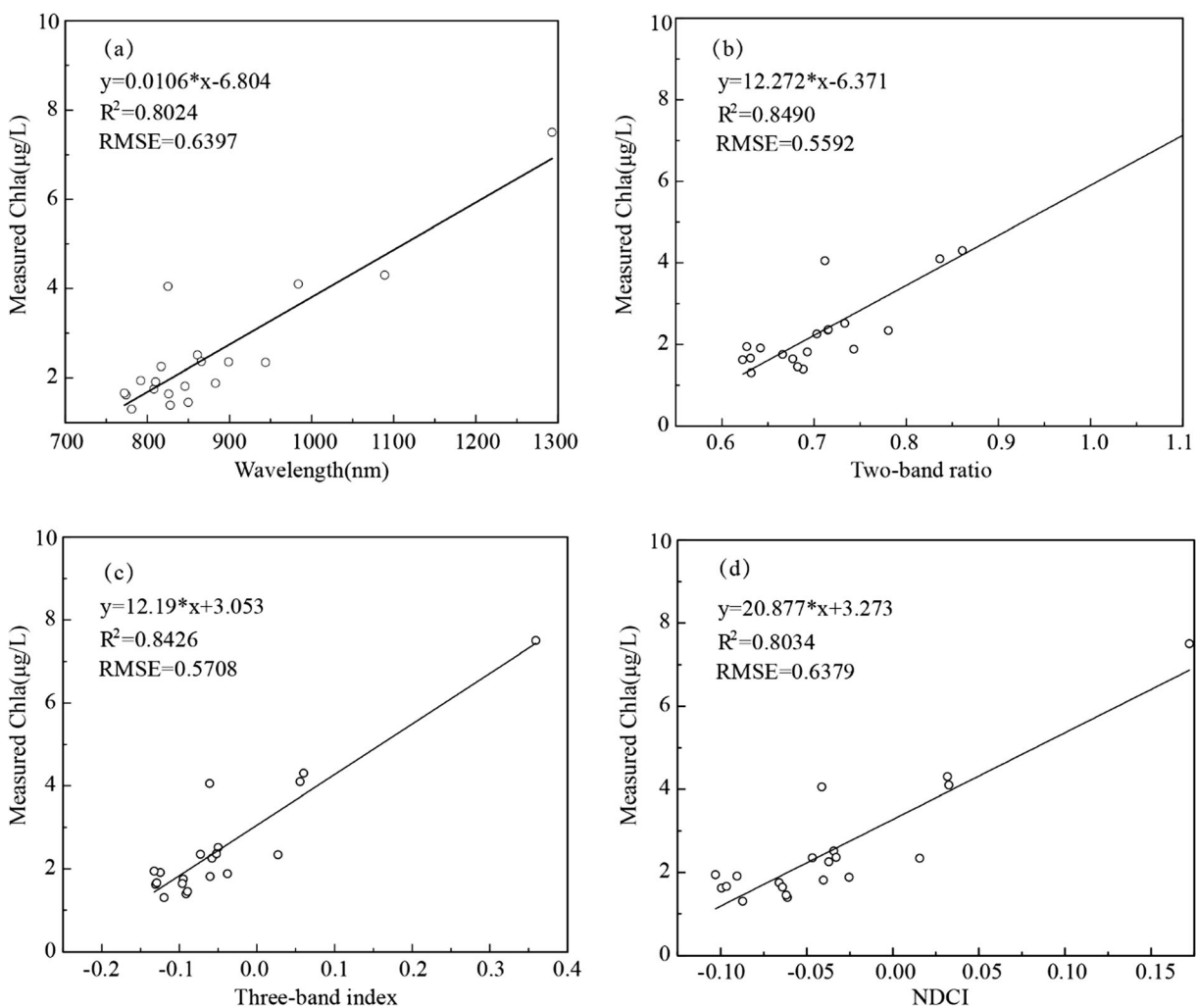


Fig. 9 Relationship between measured Chla and four algorithm indexes (a single band approach, b two band ratio approach, c the three-band approach, d NDCI)

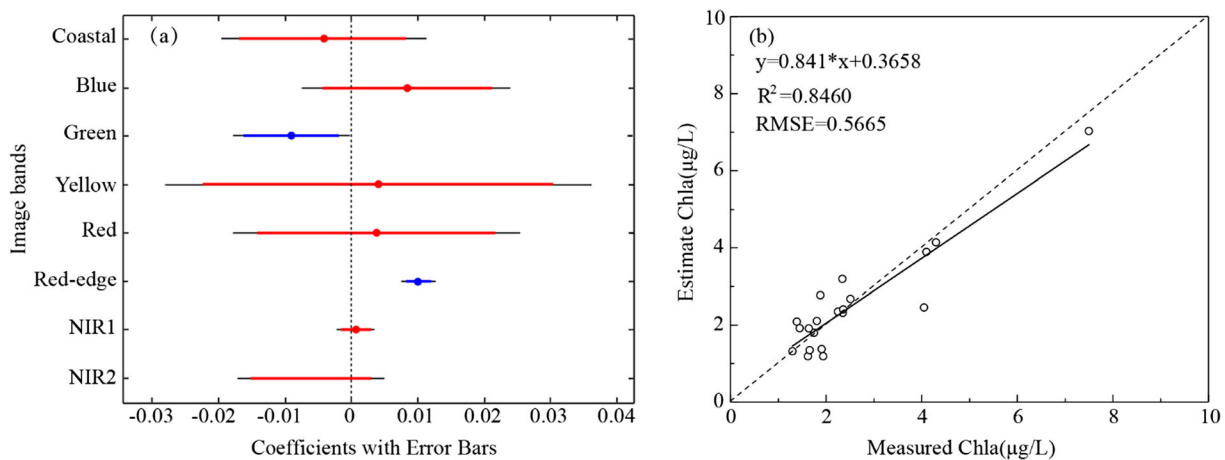


Fig. 10 **a** Stepwise regression analysis coefficients with error bars (point represents the coefficient value; blue indicates the variable introduced into the model). **b** Comparison between measured Chla

and estimated Chla derived from the stepwise regression analysis approach

From the WV-2-derived Rrs (λ) and in situ Chla data analyses, the parameterization of the first four algorithms (Fig. 9) were defined as follows:

$$\text{Single band approach: } C_{\text{chl}a} = 0.0106x - 6.804, \quad x = \text{Rrs(RedEdge)}$$

$$\text{Two-band ratio approach: } C_{\text{chl}a} = 12.272x - 6.371, \quad x = \text{Rrs(RedEdge)}/\text{Rrs(Green)}$$

$$\text{Three-band approach: } C_{\text{chl}a} = 12.19x + 3.053, \quad x = [\text{Rrs(Red)}^{-1} - \text{Rrs(RedEdge)}^{-1}] * \text{Rrs(NIR1)}$$

$$\text{NDCI } C_{\text{chl}a} = 20.877x + 3.273, \quad x = [\text{Rrs(RedEdge)} - \text{Rrs(Red)}]/[\text{Rrs(RedEdge)} + \text{Rrs(Red)}]$$

A significant correlation existed between the WV-2-derived and measured Chla ($p < 0.01$), with R^2 values of 0.802, 0.849, 0.843, and 0.803 for the single-band, two-band ratio, three-band, and NDCI approaches, respectively. The statistics confirm that the two-band ratio approach outperformed the other three approaches. A widely used algorithm, the three-band approach also showed high accuracy for estimating chlorophyll a in the WV-2 image.

In addition to the above four image band analysis approaches, we used a statistical regression method to establish the model and improve estimation accuracy.

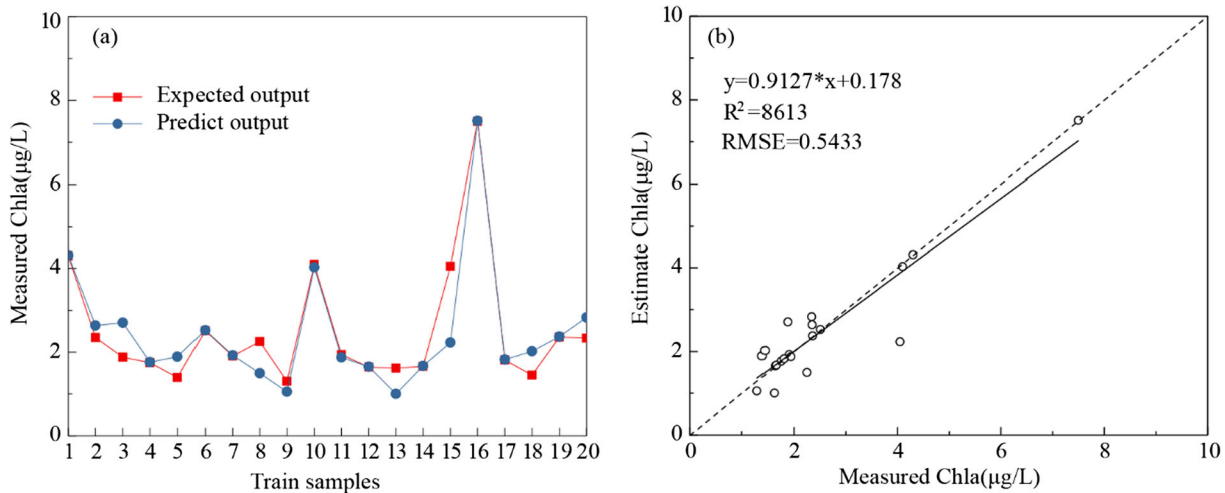


Fig. 11 **a** Model prediction results and expected output results. **b** Comparison between the Chla concentrations predicted by SVM model and measured Chla in water samples

Table 1 Accuracy assessment of Chla estimation algorithms

Chla estimation algorithms	Training samples (20 samples)				Test samples (19 samples)			
	R ²	RMSE	URMSE	P	R ²	RMSE	URMSE	P
Single-band approach	0.8024	0.6397	24.99%	<0.01	0.6895	0.6864	25.88%	<0.01
Two-band ratio approach	0.8490	0.5592	23.81%	<0.01	0.8034	0.5748	22.94%	<0.01
Three-band approach	0.8426	0.5708	22.94%	<0.01	0.7702	0.6169	22.63%	<0.01
NDCI	0.8034	0.6379	27.6%	<0.01	0.7666	0.7029	27.56%	<0.01
SRA	0.8455	0.5665	25.09%	<0.01	0.8022	0.5600	23.39%	<0.01
SVM	0.8613	0.5433	23.92%	<0.01	0.8387	0.4714	19.11%	<0.01

The significant variables of the stepwise regression algorithm are green and red edge (Fig. 10a). The parameterization of the algorithm was as follows:

$$\text{SAR} : C_{\text{chla}} = -0.009 \text{Rrs(Green)} + 0.01 \text{Rrs(RedEdge)} + 4.635$$

The R² for the stepwise regression algorithm is 0.846, and the RMSE value is 0.5665. Its estimation accuracy is lower than the two-band ratio approach.

We used the LIBSVM-3.12 library file to build the model, and experimental operating environment and platform to adopt Matlab2014b. To carry on a global search for the space with the most ideal parameters, the cross validation algorithm was selected (Chang and Lin 2011). Twenty sample points were selected for SVM training, shown in Fig. 11. The R² of the SVM approach is 0.8613 and the RMSE value is 0.5433, the highest estimation accuracy out of the six approaches.

Accuracy assessment

In addition to the accuracy assessment of the 20 training samples, we also selected 19 samples to test the extrapolation of the six approaches. Table 1 demonstrates that the *p* values of the six approaches studied in this paper are less than 0.01, confirming the statistical results are significant. Both approaches produced adequate predictions of Chla, but the two-band ratio approach and SVM have superior performance to the other approaches. For the test samples, the accuracy of the two-band ratio approach and SVM were higher than the other four approaches, with higher R² value of 0.8034 and 0.8387. SVM has the largest R² value of 0.8387, which indicates that the overall correlation between the measured Chla and SVM is highest. NDCI and single-band approach show poor estimation accuracy. Since the highest URMSE value was 27.56% for NDCI, the impact of outliers skewing

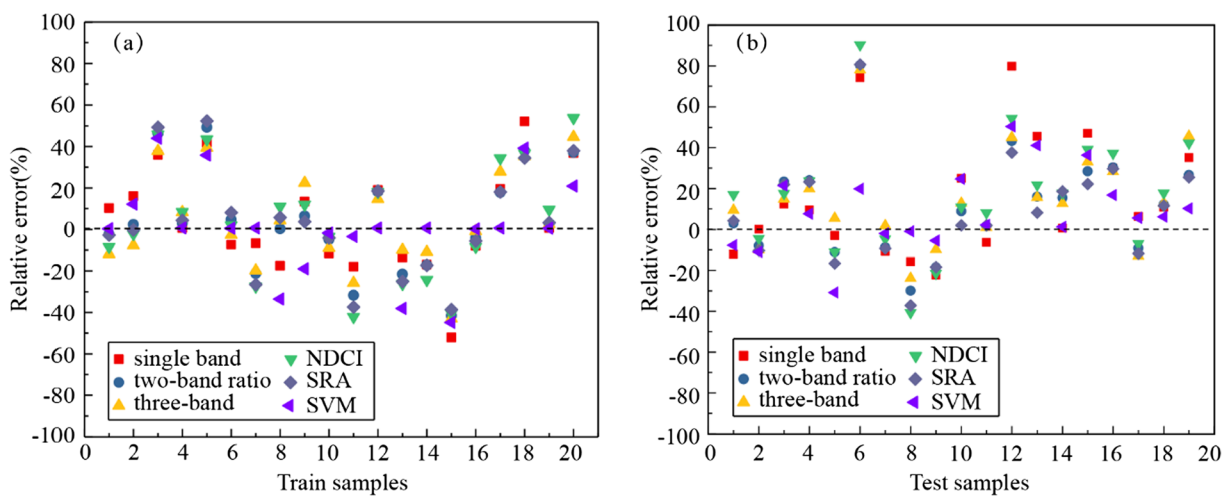


Fig. 12 Relative error distributions of the six approaches (**a** training sample, **b** test sample)

error distributions is the largest of the six approaches. Whether it is a training sample or test sample, the relative error distribution of two-band ratio and SVM is smaller (Fig. 12).

Discussion

The purpose of this paper was to evaluate the application of multispectral and high-resolution WV-2 imagery for chlorophyll a estimation in case 2 turbid waters and pinpoint a suitable approach. Experiments show that the red edge, NIR 1, and NIR 2 of WV-2 images

have a satisfactory correlation with chlorophyll a, so the image can be applied to the chlorophyll a estimation study. As for the method experiment, the two-band ratio approach, three-band approach, stepwise regression analysis algorithm, and SVM all showed sufficient estimation accuracy (Fig. 13), of which the SVM estimation of accuracy was the highest. According to the water quality monitoring data published by the Beijing Water Affairs Bureau in 2016, Guanting Reservoir has a Chla content above 10 µg/L. The predicted concentration of Chla in Guanting Reservoir has a certain degree of credibility in the published data.

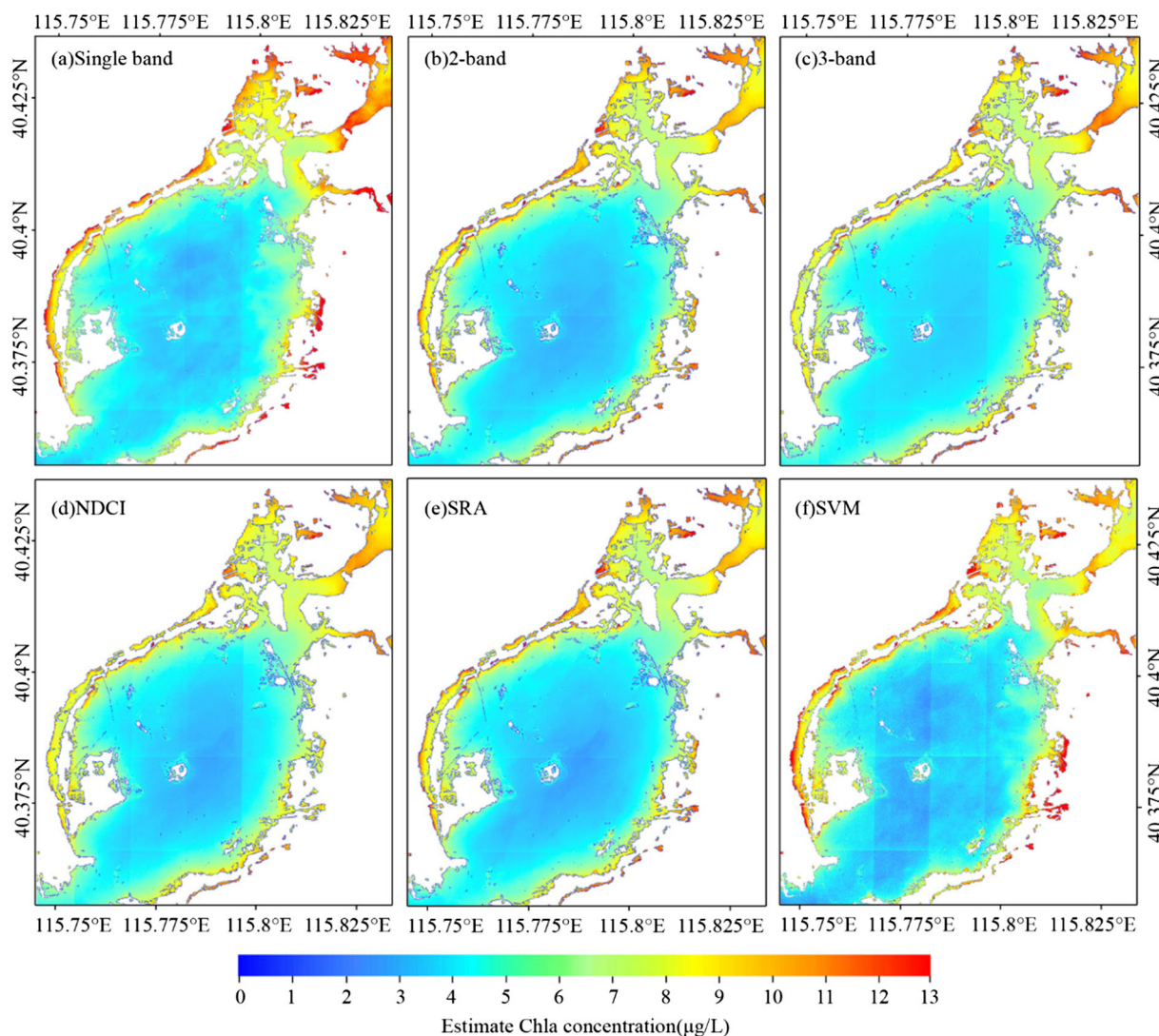


Fig. 13 Spatial distribution of chlorophyll a concentration in different estimation models. **a** Single-band model. **b** Band ratio method. **c** Three-band approach. **d** NDCI. **e** SRA. **f** SVM

Le et al. 2013 studied the Chesapeake Bay, and they found that the two-band ratio approach performed better than other approaches for MERIS; MERIS analyses indicate that the two-band ratio approach was the best method, with some limitations for low Chla ($< 2 \mu\text{g L}^{-1}$) waters. We used Guanting Reservoir as our study area, and a WV-2 image for the satellite data. By comparing different chlorophyll a algorithms, it is evident that the two-band ratio method has a higher estimation accuracy and is suitable for this study area. Two-band ratio approach reduces the effects of other non-target substances (Duan et al. 2006). The red edge and green bands were screened as significant, and had higher accuracy for estimating chlorophyll a in the band ratio approach versus the stepwise regression. Although the estimation accuracy of the three-band approach is lower than that of the two-band ratio approach, it is still passable. The three-band approach could be applied to MERIS to estimate Chla in turbid waters (Gitelson et al. 2008). We located the positions of WV-2 spectral bands and assessed the accuracy of the three band approaches. The experiments this paper describes prove that the three-band approach is suitable for the estimation of chlorophyll a in case 2 waters using WV-2 imagery.

NDCI was first proposed by Mishra and Mishra 2012 as a general index to estimate the Chla for MERIS, and it had proven successful when applied to inland coastal and estuarine waters. However, NDCI achieved lower accuracy when using WV-2 for Chla estimation. This may be due to the small number of bands of WV-2, and because MERIS is more accurate in band position selection. The sensitive bands of chlorophyll a may be relatively concentrated in the red and near-infrared regions. Hyperspectral images can be estimated with higher accuracy using the sensitive band construction models. Unfortunately, WV-2 imagery makes it difficult to accurately determine the sensitive band position since it is a wide-band image.

Sun et al. (2009) proposed a unified model based on SVM and in situ hyperspectral data for remotely estimating chlorophyll a in Lake Taihu, China. The SVM model was highly accurate, with an R^2 of 0.8961. We estimated chlorophyll a based on the SVM for WV-2 image, with the same high accuracy. SVM is advantageous since it is capable of applying information from previous examples to unknown data with higher accuracy on the training data (Sun et al. 2009).

Conclusions

There are many methods for estimating Chla in inland turbidity water. In this paper, the best algorithm for Guanting Reservoir is studied by combining WorldView-2 high-resolution multispectral images with field data. Water extraction from high-resolution images combined with spectral and spatial structure information can derive highly precise measurements of relatively pure water. In this paper, the Sobel edge detection algorithm and NDWI were used to extract water bodies, excluding aquatic plants and other interferences (including motor boats, cruise ships, and wind power generation towers). The relationship between the measured Chla concentration and the measured turbidity value was correlated with the ASD-measured water spectrum and the WorldView-2 image bands. The analysis showed that Chla concentration had a high correlation in the red and near-infrared regions. The correlation between the turbid water and the coastal band of the WorldView-2 image is high, while the correlation between Chla and coastal band is low, which suggests that the application of the coastal band is different from the case 1 waters.

Of the six Chla estimation approaches, SVM is the most suitable for Guanting Reservoir because of its higher estimation accuracy. SVM does not consider the complexity of the water environment, is more applicable, and has higher accuracy. However, the SVM algorithm has a greater dependency on the measured data, and the optimization method of the algorithm parameters still needs improvement. In the future, these issues will be addressed and the accuracy of SVM will be further enhanced.

Funding information This research was financially supported by the International Science & Technology Cooperation Program of China (Grant no.2014DFA21620).

References

- Chang, C. C., & Lin, C. J. (2011). LIBSVM: A library for support vector machines. *ACM*, 2(3), 1–27. <https://doi.org/10.1145/1961189.1961199>.
- Chen, Y., Shi, R., Shu, S., & Gao, W. (2013). Ensemble and enhanced pm 10, concentration forecast model based on stepwise regression and wavelet analysis. *Atmospheric Environment*, 74(74), 346–359. <https://doi.org/10.1016/j.atmosenv.2013.04.002>.

- Dall'Olmo, G., & Gitelson, A. A. (2005). Effect of bio-optical parameter variability on the remote estimation of chlorophyll-a concentration in turbid productive waters: Experimental results. *Applied Optics*, 44(3), 412–422. <https://doi.org/10.1364/AO.44.000412>.
- Dall'Olmo, G., & Gitelson, A. A. (2006). Effect of bio-optical parameter variability and uncertainties in reflectance measurements on the remote estimation of chlorophyll-a concentration in turbid productive waters: Modeling results. *Applied Optics*, 45(15), 3577–3592. <https://doi.org/10.1364/AO.45.003577>.
- Dall'Olmo, G., Gitelson, A. A., Rundquist, D. C., Leavitt, B., Barrow, T., & Holz, J. C. (2005). Assessing the potential of seawifs and modis for estimating chlorophyll concentration in turbid productive waters using red and near-infrared bands. *Remote Sensing of Environment*, 96(2), 176–187. <https://doi.org/10.1016/j.rse.2005.02.007>.
- DigitalGlobe (2009). The benefits of the 8 spectral bands of WorldView-2. http://worldview2.digitalglobe.com/docs/WorldView-2_8Band_Applications_Whitepaper.pdf. Accessed 20 July 2011.
- Duan, H., Lei, Y. U., Zhang, B., Liu, D., & Song, K. (2006). Hyperspectral data applied in monitoring and evaluating the water trophic state of Lake Chagan. *Acta Scientiae Circumstantiae*, 26(7), 1219–1226.
- Gitelson, A. (1992). The peak near 700 nm on radiance spectra of algae and water: Relationships of its magnitude and position with chlorophyll concentration. *International Journal of Remote Sensing*, 13, 3367–3373. <https://doi.org/10.1080/01431169208904125>.
- Gitelson, A. A., Dall'Olmo, G., Moses, W., Rundquist, D. C., Barrow, T., Fisher, T. R., Gurlin, D., & Holz, J. (2008). A simple semi-analytical model for remote estimation of chlorophyll-a, in turbid waters: Validation. *Remote Sensing of Environment*, 112(9), 3582–3593. <https://doi.org/10.1016/j.rse.2008.04.015>.
- Gons, H. J. (1999). Optical teledetection of chlorophyll a in turbid inland waters. *Environmental Science & Technology*, 33(7), 1127–1132. <https://doi.org/10.1021/es9809657>.
- Gons, H. J., Rijkeboer, M., & Ruddick, K. G. (2005). Effect of a waveband shift on chlorophyll retrieval from meris imagery of inland and coastal waters. *Journal of Plankton Research*, 27(1), 125–127. <https://doi.org/10.1093/plankt/fbh151>.
- Goodin, D. G., Han, L., Fraser, R. N., Rundquist, D. C., Stebbins, W. A., & Schalles, J. F. (1993). Analysis of suspended solids in water using remotely sensed high resolution derivative spectra. *Photogrammetric Engineering & Remote Sensing*, 59(4), 505–510.
- Gordon, H. R., & Morel, A. Y. (1983). Remote assessment of ocean color for interpretation of satellite visible imagery. *Physics of the Earth & Planetary Interiors*, 37(4), 292. [https://doi.org/10.1016/0031-9201\(85\)90018-4](https://doi.org/10.1016/0031-9201(85)90018-4).
- Han, L. H., & Rundquist, D. C. (1997). Comparison of NIR/RED ratio and first derivative of reflectance in estimating algal-chlorophyll concentration: A case study in a turbid reservoir. *Remote Sensing of Environment*, 62, 253–261. [https://doi.org/10.1016/S0034-4257\(97\)00106-5](https://doi.org/10.1016/S0034-4257(97)00106-5).
- Hooker, S. B., Lazin, G., Zibordi, G., & Mclean, S. (2002). An evaluation of above- and in-water methods for determining water-leaving radiances. *Journal of Atmospheric & Oceanic Technology*, 19(4), 486–515. [https://doi.org/10.1175/1520-0426\(2002\)019<0486:AOAAI>2.0.CO;2](https://doi.org/10.1175/1520-0426(2002)019<0486:AOAAI>2.0.CO;2).
- Jiao, H. B., Zha, Y., Gao, J., Li, Y. M., Wei, Y. C., & Huang, J. Z. (2006). Estimation of chlorophyll-a concentration in Lake Tai, China using in situ hyperspectral data. *International Journal of Remote Sensing*, 27(19), 4267–4276. <https://doi.org/10.1080/01431160600702434>.
- Kirk, J. T. O. (1994). *Light and photosynthesis in aquatic ecosystems*, 2nd Edition [M]. Cambridge: Cambridge University Press.
- Laben, C. A., & Brower, B. V. (2000). Process for enhancing the spatial resolution of multispectral imagery using pan-sharpening. *Websterny Uspevnyi*.
- Le, C., Hu, C., Cannizzaro, J., English, D., Muller-Karger, F., & Lee, Z. (2013). Evaluation of chlorophyll-a remote sensing algorithm for an optically complex estuary. *Remote Sensing of Environment*, 129(2), 75–89. <https://doi.org/10.1016/j.rse.2012.11.001>.
- Le, C. F., Li, Y. M., Yong, Z., Sun, D. Y., Huang, C. C., & Lu, H. (2009). A four-band semi-analytical model for estimating chlorophyll a in highly turbid lakes: The case of Taihu Lake, China. *Remote Sensing of Environment*, 113(6), 1175–1182. <https://doi.org/10.1016/j.rse.2009.02.005>.
- Lin, C., Wu, C. C., Tsogt, K., Ouyang, Y. C., & Chang, C. I. (2015). Effects of atmospheric correction and pansharpening on LULC classification accuracy using WorldView-2 imagery. *Information Processing in Agriculture*, 2(1), 25–36. <https://doi.org/10.1016/j.inpa.2015.01.003>.
- Manakos, I., Manevski, K., Kalaitzidis, C., & Edler, D. (2011). Comparison between FLAASH & ATCOR atmospheric correction modules on the basis of WorldView-2 imagery and in situ spectroradiometric measurements. Earsel, Sig-Imaging Spectroscopy Workshop.
- Mcfeeters, S. K. (1996). The use of the normalized difference water index (ndwi) in the delineation of open water features. *International Journal of Remote Sensing*, 17(7), 1425–1432. <https://doi.org/10.1080/01431169608948714>.
- Mishra, S., & Mishra, D. R. (2012). Normalized difference chlorophyll index: A novel model for remote estimation of chlorophyll-a, concentration in turbid productive waters. *Remote Sensing of Environment*, 117(2), 394–406. <https://doi.org/10.1016/j.rse.2011.10.016>.
- Mobley, C. D. (1994). Light and water: Radiative transfer in natural waters. Academic Press.
- O'Reilly, J. E., Maritorena, S., Mitchell, B. G., Siegel, D. A., Carder, K. L., Garver, S. A., Kahru, M., & McClain, C. (1998). Ocean color chlorophyll algorithms for seawifs. *Journal of Geophysical Research Oceans*, 103(C11), 24937–24953. <https://doi.org/10.1029/98JC02160>.
- Pu, R., & Landry, S. (2012). A comparative analysis of high spatial resolution IKONOS and WorldView-2 imagery for mapping urban tree species. *Remote Sensing of Environment*, 124(9), 516–533. <https://doi.org/10.1016/j.rse.2012.06.011>.
- Schalles, J. F. (2006). Optical remote sensing techniques to estimate phytoplankton chlorophyll a concentrations in coastal. *Remote sensing of aquatic coastal ecosystem processes*.
- Sun, D. Y., Li, Y. M., & Qiao, W. (2009). A unified model for remotely estimating chlorophyll a in Lake Taihu, China, based on SVM and in situ hyperspectral data. *IEEE Transactions on Geoscience & Remote Sensing*, 47(8), 2957–2965. <https://doi.org/10.1109/TGRS.2009.2014688>.
- Tang, J., Tian, G., Wang, X., Wang, X., & Song, Q. (2004). The methods of water spectra measurement

- and analysis I: Above-water method. *Journal of Remote Sensing*, (01):37–44.
- Vapnik, V. (1996). Support vector method for function approximation, regression estimation, and signal processing. *Advances in Neural Information Processing Systems*, 9, 281–287.
- Wang, J. (2013). *Pearson correlation coefficient*. Springer New York, Pearson Correlation Coefficient.
- Wang, X. L., Zhou, Z. Y., & Yan, J. P. (2009). Apply GA-SVM to retrieve water quality parameters of Weihe River from multispectral remote sensing data. *Journal of Remote Sensing*, 13(4), 735–744.
- Yacobi, Y. Z., Moses, W. J., Kaganovsky, S., Sulimani, B., Leavitt, B. C., & Gitelson, A. A. (2011). Nir-red reflectance-based algorithms for chlorophyll- a, estimation in mesotrophic inland and coastal waters: Lake Kinneret case study. *Water Research*, 45(7), 2428–2436. <https://doi.org/10.1016/j.watres.2011.02.002>.
- Zhang, Y., Ma, R., Duan, H., Loiselle, S., Zhang, M., & Xu, J. (2016). A novel MODIS algorithm to estimate chlorophyll a concentration in eutrophic turbid lakes. *Ecological Indicators*, 69, 138–151. <https://doi.org/10.1016/j.ecolind.2016.04.020>.
- Zhen, Z., Gong, Z. N., & Zhao, W. J. (2012). Analysis of hydrophytes for spatial evolution pattern in Guanting Reservoir, China. *Journal of Agro-Environment Science*, 31(8), 1586–1595.
- Zhou, Y., Zhou, W. Q., Wang, S. X., & Zhang, P. (2004). Applications of remote sensing techniques to inland water quality monitoring. *Advances in Water Science*, 15(3), 312–317.
- Zhu, X., Zhang, H., Lei, P., Zhang, B., Shan, B., & Shi, M. (2015). Historical distribution characteristics of major elements in Guanting Reservoir sediment. *Huanjing Kexue Xuebao* 36(2). <https://doi.org/10.13671/j.hjkxxb.2015.0475>.